



OPEN

Anti-proliferative activity, molecular genetics, docking analysis, and computational calculations of uracil cellulosic aldehyde derivatives

Asmaa M. Fahim^{1✉}, Sawsan Dacrory² & Ghada H. Elsayed^{3,4}

In this study, the oxidation of microcrystalline cellulose using NaIO_4 to yield the corresponding cellulose aldehyde utilized microwave irradiation as a green tool, the obtained cellulosic aldehyde was confirmed through spectral analysis and it has an active site to react with the synthesized uracil acetamide to afford the corresponding arylidene cellulosic MDAU(4), the latter compound which can easily due to presence of active $\text{CH}=\text{O}$ group behind a cyano group react with nitrogen nucleophile's and cyclized with hydrazine hydrate to give pyrazole cellulosic MDPA(5). The spectral analysis of the obtained cellulosic derivatives was confirmed with FT-IR, NMR, and SEM. Additionally, a neutral red uptake analysis has been used to investigate the cytotoxic activity of the cellulosic compounds MDAC(2), MDAU(4), and MDAP(5) against the cancer cells A549 and Caco2. After 48 h, Compound MDAU(4) had a stronger inhibitory effect on the growth of A549 and Caco2, compared to control cells. Then, using QRT-PCR, the expression levels of the genes β -Catenin, c-Myc, Cyclin D1, and MMP7 in A549 cells were examined. By reducing the expression levels of the Wnt signaling cascade genes (β -Catenin, c-Myc, Cyclin D1, and MMP7) when administered to A549 cells, compound MDAU(4) was shown in this investigation to be a viable candidate compared to lung cancer. Additionally, docking simulation was used to explore the uracil cellulosic heterocycles attached to different proteins, and computational investigations of these compounds looked at how well their physical characteristics matched the outcomes of their experiments.

The waste minimization of agriculture waste takes the attention of most scientists due to the presence of cellulosic waste which has chains comprised $\beta(1 \rightarrow 4)$ linked to D-glucose¹⁻⁵ and have different hydrogen bonding interactions, that are active in biological estimation for instance bio adhesive drug delivery systems^{3,6-8}. Furthermore, Lung cancer is one of the maximum popular cancers internationally, and it is disturbing in males and females^{9,10}. Wnt/ β -catenin signaling pathway is an important molecular cascade in modified embryonic development and adult homeostasis¹¹⁻¹⁴. However, it has been implicated in multiple human malignancies, including colorectal cancer, breast cancer, prostate cancer, and non-small cell lung cancer, due to dysregulation¹⁵⁻¹⁸. Beta-catenin is one of a big and complicated array of proteins which it's involved in the control of the Wnt/ β -catenin signaling pathway^{18,19}. Also, the dissociation of beta-catenin from this destruction complex outcomes in the aggregation of beta-catenin in the cytoplasm and nucleus, which activates the target genes of the Wnt pathway, such as cyclin D1, MMP7, and c-Myc in human cancers^{20,21}. In this elucidation, we synthesized the novel pyrazole cellulosic compounds from the reaction of condensation with cellulose aldehyde with active CN-uracil acetamide to give the corresponding cellulose arylidene MDAU(4). This compound can then be

¹Green Chemistry Department, National Research Centre (NRC), P.O. Box 12622, DokkiCairo, Egypt. ²Cellulose and Paper Department, National Research Centre, P.O. Box 12622, Giza, Egypt. ³Department of Hormones, National Research Centre (NRC), P.O. Box 12622, Dokki, Giza, Egypt. ⁴Stem Cells Lab, Center of Excellence for Advanced Sciences, National Research Centre (NRC), P.O. Box 1262, Dokki, Giza, Egypt. ✉email: am.abdel-wahid@nrc.sci.eg; asmaamahmoud8521@gmail.com

easily cyclized in the presence of nitrogen nucleophiles like hydrazine hydrate to give the pyrazole cellulosic derivative **MDAP(5)**, which was confirmed through spectral analysis. Additionally, we examined these cellulosic derivatives with cytotoxic effects on lung cancer cells (A549) and colon cancer cells (Caco2), and we then examined the levels of β -Catenin, c-Myc, Cyclin D1, and MMP7 gene expression in A549 cells. The heterocyclic cellulosic compounds were also docked with the **PDBID:2ito**, 1nun, 5jsn, and 5vzu, respectively. Additionally, the cellulosic compounds were improved utilized the DFT/B3LYP/6-311(G) basis set, which demonstrated the stability of the compounds as a result of the interaction of the NH and OH of cellulose, uracil, and pyrazole in electrostatic hydrogen bonds^{14,22–24}.

Experimental section

Apparatus

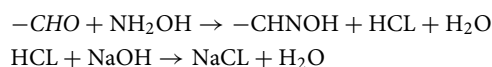
The Shimadzu FT-IR 8101 PC infrared spectrophotometer recorded the IR spectra. The ¹H NMR and ¹³C NMR spectra were determined in DMSO-d₆ at 300 MHz on a Varian Mercury VX 300 NMR spectrometer (¹H at 300 MHz, ¹³C at 75 MHz) exhausting trimethyl silane as an internal typical. Scanning electron microscopes (SEM) were investigated utilizing JEOL JXA-840A electron probe Microanalyzer Company and were air-dried before imaging, and images were obtained using an accelerating voltage of 10–15 kV. In closed vessels under pressure, microwave-irradiated Pyrex tubes with caps were used to conduct the reactions.

Reagent

Microcrystalline cellulose (20 μ m) was obtained from the Rasyan research laboratory, and NaIO₄ was ordered from Fluka. EtOH, NH₂NH₂, triethyl amine, purchased from Aldrich Chemical Company. 2-cyano-*N*-(2,4-dioxo-1,2,3,4-tetrahydropyrimidin-5-yl)acetamide(3) was synthesized according previous procedure²⁵.

Synthesis of cellulose aldehyde MDAC(2)

Using a microwave device, cellulose was oxidized to various degrees of oxidation with NaIO₄ (20 ml). At 3, 1, and 1.5 min, the precursor was transferred to the microwave to finish the oxidation process. The oxidized product was filtered, EtOH washed, and allowed to dry for a whole night at room temperature. Using 1.5 g of cellulose and 20 ml of distilled water, aldehyde concentration was determined²⁶, through the basic response of Schiff. NH₂OH.HCl is used when aldehyde groups transform into oximes. Dialdehyde cellulose, 0.3 g, was dispersed in 20 ml of pH-5 NaOH solution-containing water, then, NH₂OH.HCl (0.72 mol/l) was added at pH 5 for 4 hours, the mixture was stimulated at 40 °C. To titrate the emitted HCl, a 1.0 M aqueous NaOH solution was used. The volume of alkali solution consumed during the titration was recorded (in liters), and the amount of NaOH consumed when the pH value of the solution reached 5.0 was validated. The volume of 1.0 M sodium hydroxide solution consumed was measured as Vc (in liters), using the same concentration of cellulose solution at pH 5.0 as a blank. The following equation is used to designate the aldehyde content (% w/w)^{27,28}.



$$\text{Aldehyde content}(\%)t = \frac{C(\text{NaOH}) \cdot Va - VC}{8 \text{ mM}}$$

where C_{NaOH} = 1.0 M, m is the dry weight of DAC (0.3 g) used in the experiment, and M molecular weight of the repeating unit of cellulose (162).

Reaction of MDAC(2) with synthesized 2-cyano-*N*-(2,4-dioxo-1,2,3,4-tetrahydropyrimidin-5-yl)acetamide(3)

Stirring solution of MDAC(2) (1 g, 10 mmol) was mixed with 2-cyano-*N*-(2,4-dioxo-1,2,3,4-tetrahydropyrimidin-5-yl)acetamide(3)(1 g, 10 mmol) in EtOH and 2 drops of triethylamine as basic catalyst were refluxed for 5 h at 120 °C and monitored through TLC with (ethyl acetate/petroleum ether) eluent(1:1) then the product filtered off and recrystallized from EtOH/H₂O to afford the corresponding (*Z*)-2-cyano-*N*-(2,4-dioxo-1,2,3,4-tetrahydropyrimidin-5-yl)-5,7-dihydroxy-6-(1-hydroxy-2-oxoethoxy)hept-2-enamide (4): colorless powder, m.p = > 300 °C, FT-IR (KBr): ν 3410(OH), 3352(NH), 3200(NH), 3174(NH), 2990 (CH₂), 1650(C=O), 1550(C=C); ¹H-NMR (DMSO-d₆): δ 3.54(m, CH₂, glybose), 4.02(m, OH), 6.6 (d, H, CH), 7.02(d, H, CH), 7.9 (H, s, CH), 7.5 (m, H, CH), 8.96 (s, NH uracil, D₂O exchangeable), 10.32(s, CH=) 11.62(NH, D₂O exchangeable), ¹³CNMR(DMSO-d₆), δ 28(CH₂), 66(CH₂), 77(CH₂), 88(CH₂), 100 (CH=), 110(CH), 115(CN), 134(CH), 150(CH=), 160(C=O), 169(CH=).

Synthesis of MDUP(5)

Reactivity of MDAU(4) (0.368 g, 1 mmol) with hydrazine hydrate (1 mmol) was heated for 6 h, then left to cool and monitored through TLC with (ethyl acetate/petroleum ether) eluent (1:1) then the product was formed and filtered off, washed with ethanol, and dried. Recrystallization from DMF/H₂O to give 3-amino-5-(1,3-dihydroxy-2-(1-hydroxy-2-oxoethoxy)propyl)-*N*-(2,4-dioxo-1,2,3,4-tetrahydropyrimidin-5-yl)-1H-pyrazole-4-carboxamide(5): yellow powder, m.p = > 300 °C, FT-IR (KBr): ν 3455(OH), 3400(OH), 3364(NH), 3305(NH), 3214(NH), 3204(NH), 3175(NH₂), 2990 (CH₂), 1715(C=O), 1655(C=O), 1599(C=O), 1510(C=C), ¹H-NMR (DMSO-d₆): δ 3.65(m, CH₂, glybose), 4.11(s, OH, D₂O exchangeable), 5.21 (s, OH, D₂O exchangeable), 6.35 (d, NH₂, D₂O exchangeable), 7.5 (d, H, CH), 9.52 (1H, s, NH exchangeable), 10.02(s, OH, D₂O exchangeable), 11.20

(s, NH D₂O exchangeable), 11.52(s, NH, exchangeable), 12.01(s, NH, exchangeable), ¹³CNMR(DMSO-d₆), δ 55(CH₂), 84(CH₂), 100(CH₂), 112(CH), 135(CH), 141(CH), 155(C=O), 160(C=O), 164(C=O), 177(C=O).

Cytotoxicity screening

A549 and **Caco2** cell lines were acquired from American Type Culture Collection and conserved in suitable conditions. **A549** cells were refined in DMEM (Dulbecco's modified Eagle's Medium) and **Caco2** cells were cultured in RPMI Medium containing 10% fetal bovine serum (FBS), 100 U/ml penicillin, and 100 µg/ml streptomycin sulfate at 37 °C in a humidified 5% CO₂. The cells were digested with 0.025% trypsin-EDTA for passaging. The cells in the logarithmic growth phase were used in the experiment. The cytotoxicity of uracil pyrazole cellulosic compounds was examined via a neutral red uptake method. Several concentrations (6.25, 12.5, 25, 50, 100, and 200 µM) of heterocycles were added to continue the culture for 48 hours at a cell density of 10⁴ cells/well of 96 well plate and neutral red uptake assay was done as reported by Repetto et al.²⁹. The relative between the used log concentrations and the neutral red intensity value accustomed estimate half maximal inhibitory concentration (IC₅₀) of heterocycles. The medium was added instead of the cellulosic heterocycles for the untreated cells (negative control). A cytotoxic natural agent (doxorubicin, Mr = 543.5) was used as positive control giving 100% inhibition. Cellulose products were dissolved in DMSO and its final concentration was not increased than 0.2% in the cells. All analyses were achieved at least three times.

Gene expression analysis

Quantitative real-time PCR

RNA was isolated from **A549** cells (3 × 10⁴ cells/well) and treated for 48 h using RNA easy mini Kit (Qiagen, USA) then the concentration and purity of total extracted RNA were determined using NanoDrop one micro-volume UV spectrophotometer (Thermo Fisher Scientific, USA). RNA of each treatment was converted to first-strand cDNA according to manufacturer instructions using Revert Aid First Strand cDNA Synthesis Kit (Thermo Scientific, USA). Specific primer sequences are listed in Table 1. Expression levels of *β-Catenin*, *c-Myc*, *Cyclin D1*, and *MMP7* genes were normalized concerning *β-actin* transcript using Maxima SYBR Green qPCR Master Mix (2X) (Thermo Scientific, USA) and calculated by 2^{-ΔΔCT} method⁵⁹. The reaction conditions were as follows: 95 °C for 10 min, 95 °C for 15 s, 60 °C for 30 s and 72 °C for 30 s with a total of 40 cycles of amplification. DNA Technology Detecting Thermocycler DT Lite 4S1 was used for gene expression quantitation.

Statistical evaluation

Outcomes are expressed as Mean ± SEM. Statistical analyses of the data are achieved utilizing Sigma plot ver. 125. A student t-test was used to analyses of the data and find the examined compounds' significant differences. Changes were considered significant when *P* < 0.05.

Molecular docking studies

Dockage of uracil cellulosic heterocycles using the MOE program³⁰ to confirm the biological action and communication with them concluded different binding proteins such as Crystal structure of EGFR kinase domain G719S mutation in complex with Iressa (PDBID:2ito)³¹, Crystal Structure Analysis of the FGFR1-FGFR2b Complex (PDBID:1nun)³², Bcl2-inhibitor complex (PDB ID: 5jsn)³³ and Crystal structure of the Skp1-FBXO31-cyclin D1 complex (PDB ID: 5vzu)³⁴, correspondingly. For separate proteins, 9 dissimilar docking simulations were operate utilized default limits^{3,35}.

DFT optimization

Uses of the gas phase of DFT/B3LYP/6-311(G) level utilized Gaussian 09 program³⁶ was used for the geometry optimization^{37,38}. The majority benefit of DFT methods is that they afford a substantial growth in computational accurateness lacking increasing computation time. All chemicals were imagined via Gauss-View³⁹. Physical limitations were evaluated using the E_{HOMO} and E_{LUMO} values, while other limitations were retrieved from files^{40,41}.

Results section

Chemistry part

Oxidation of microcrystalline cellulosic ring MCEC(1) with sodium hypochlorite utilized Microwave irradiation MDAC(2) in excellent yield, the formation of cellulose aldehyde MDAC(2) was confirmed through previous studies^{28,42} and determination of cellulose aldehyde content, the reactivity of cellulose aldehyde MDAC(2) was so reactive which has methyl group which easily of attack with any active methylene group, as displayed in

Gene	Primer forward (5'-3')	Primer reverse (5'-3')
β-actin	CCTTCCTGGGCATGGAGTCCT	GGAGCAATGATCTTGATCTTC
β-Catenin	TAGAAACAGCTCGTTGTACCGCTGGGACCT	GCACTGCCATTTAGCTCCTTCTTGATGTAAT
c-Myc	AGAGAAGCTGGCCTCCTACC	CGTCGAGGAGAGCAGAGAAT
Cyclin D1	GCTGCGAAGTGGAAACCATC	CCTCCTTCTGCACACATTTGAA
MMP7	GTGGTCACCTACAGGATCGTA	CTGAAGTTTCTATTCTTCTTCTGA

Table 1. Primer sequences used in the RT-PCR investigation.

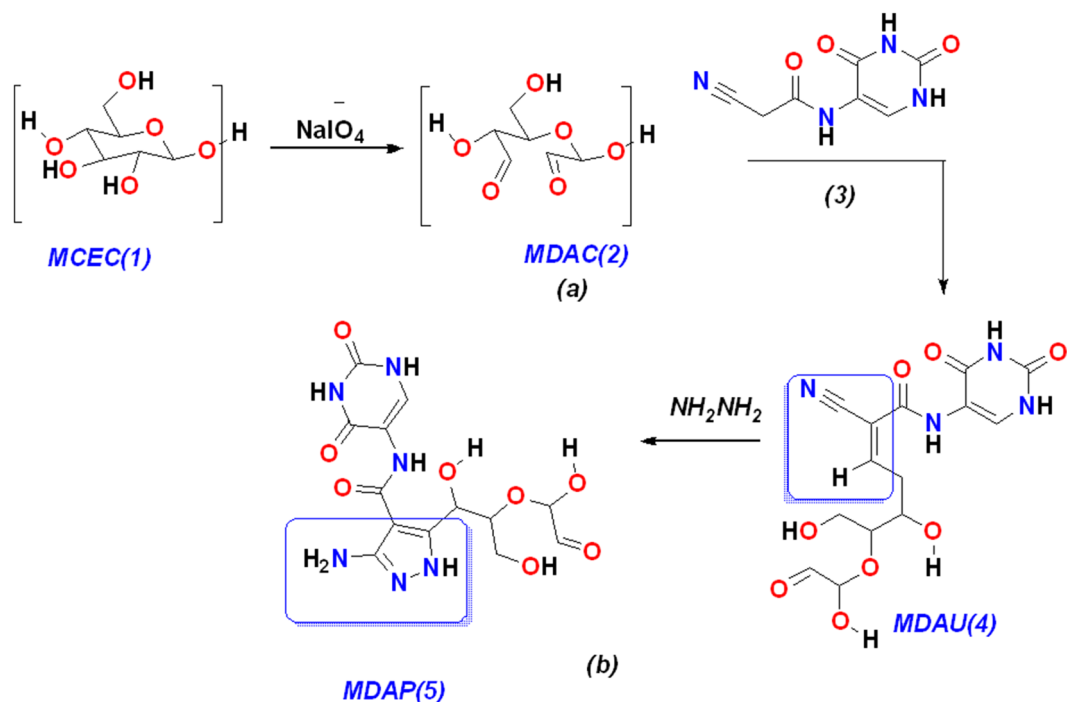


Figure 1. (a) Formation of cellulose aldehyde via oxidation (b) Reaction of MDAC with acetamide and formation of MDAP(5).

Fig.1(a). Furthermore, the reaction of MDAC(2) with 2-cyano-*N*-(2,4-dioxo-1,2,3,4-tetrahydropyrimidin-5-yl)acetamide(3) in equal amounts to afford the corresponding (*Z*)-2-cyano-*N*-(2,4-dioxo-1,2,3,4-tetrahydropyrimidin-5-yl)-5,7-dihydroxy-6-(1-hydroxy-2-oxoethoxy)hept-2-enamide MDAU(4) and confirmed through FT-IR which showed 3410 cm⁻¹ for hydroxyl group and more NH group at 3352–3174 cm⁻¹ due to presence of uracil moiety and 2250 cm⁻¹ for C≡N group, also the ¹HNMR showed CH=olefin hydrogen of arylidene at δ = 10.32 ppm and more exchangeable proton at OH and NH of glycoside and uracil moieties at 4.02, 8.96, 11.62 ppm; respectively. Furthermore, the reactivity of arylidene MDAU(4) due to the presence of olefin hydrogen adjacent to the C≡N group which can be easy to cyclized in the presence of nitrogen nucleophiles such as NH₂NH₂, also the reactivity of MDAU(4) with hydrazine hydrate refluxing in EtOH to afford the corresponding 3-amino-5-(1,3-dihydroxy-2-(1-hydroxy-2-oxoethoxy)propyl)-*N*-(2,4-dioxo-1,2,3,4-tetrahydro pyrimidin-5-yl)-1*H*-pyrazole-4-carboxamide MDAP(5) and showed the stretching absorption band at 3175 cm⁻¹ for an amino

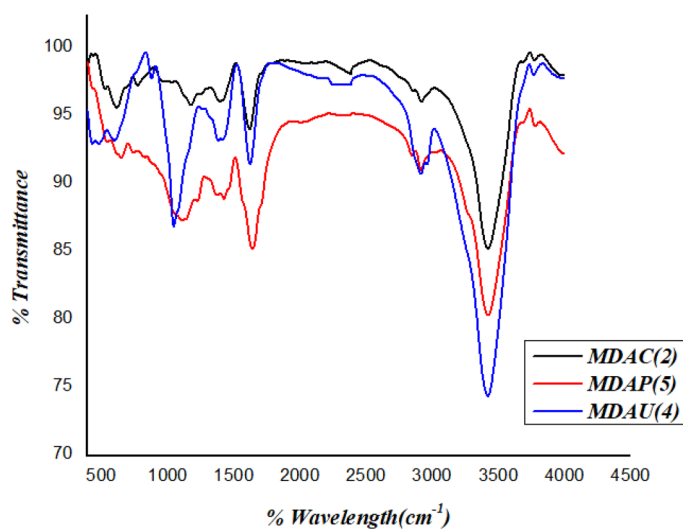
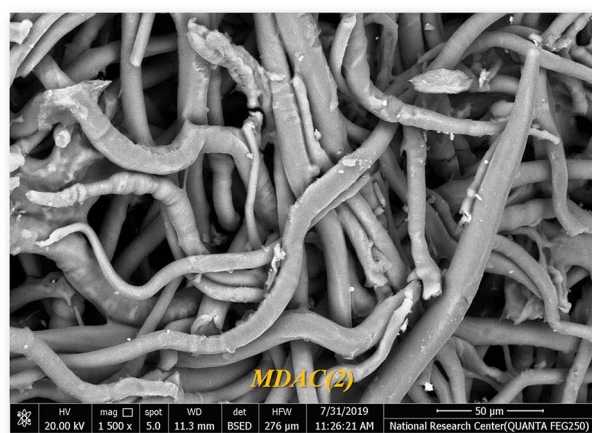
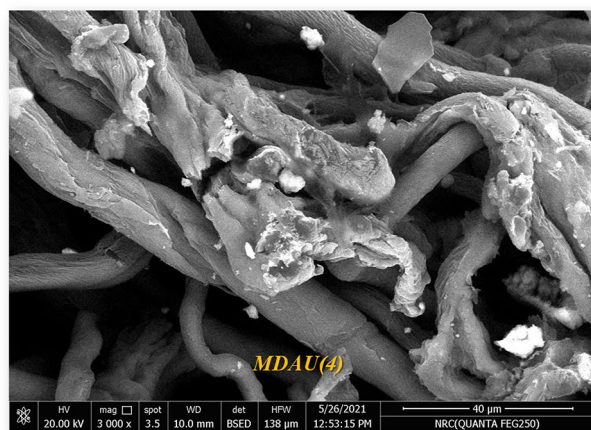


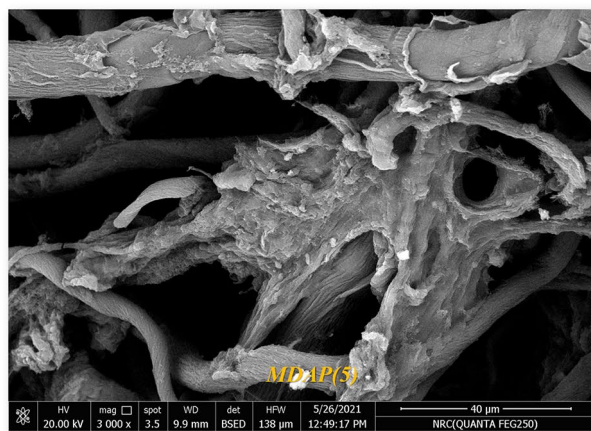
Figure 2. FT-IR of synthesized MDAC(2), MDAU(4) and MDAP(5); respectively.



(A) MDAC



(B)MDAU(4)



(C) MDAP(5)

Figure 3. (A–C): SEM morphology of MDAC, MDAU and MDAP; respectively.

group of the pyrazole ring and more of NH bands at $3364\text{--}3204\text{ cm}^{-1}$ and the NMR showed exchangeable protons of NH_2 group at 11.20 ppm and the NH protons were deshielded in 11.52, 12.01 ppm, and the ^{13}C NMR showed the three carbonyl bonds from the range at $155\text{--}177\text{ ppm}$; respectively as demonstrated in Fig. 1(b).

IR characterization

FT-IR of the novel synthesized cellulosic heterocycles was cellulose aldehyde MDAC(2), arylidine MDAU(4), and Pyrazole cellulose MDAP(5) as displayed in Figure 2. The compound MDAC(2) showed a characteristic absorption band of $\text{C}=\text{O}$ at 1650 cm^{-1} represents to two aldehyde group, and these bands can be so small

A549 cells		Caco2 cells	
Compounds	IC ₅₀ (μM)	Compounds	IC ₅₀ (μM)
MDAC(2)	59	MDAC(2)	188.8
MDAU(4)	17.3	MDAU(4)	89.26
MDAP(5)	89.7	MDAP(5)	150.24
Doxorubicin	4.8	Doxorubicin	22.54

Table 2. The cytotoxicity activity of heterocycles on **A549** and **Caco2** cells. IC₅₀: Concentration required to inhibit cell viability through 50%.

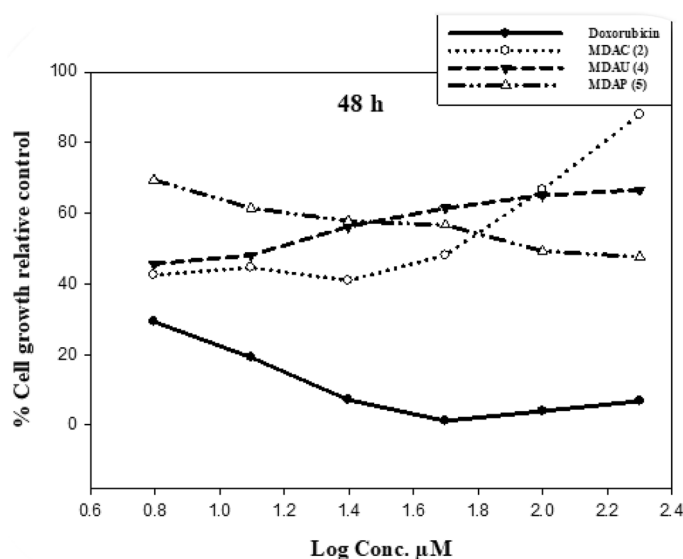


Figure 4. Outcome of cellulosic compounds on **A549** cells at 48 h.

or hidden in hydrated form but there is hemiacetal group which confirms the presence of aldehyde group. Furthermore, the presence of an adsorption band at 800–750 cm⁻¹ conforms to the hemiacetal bond which is a typical peak of aldehyde^{26,28}. Moreover, the MDAU(4) showed a characteristic beak of the presence of three NH bands in the range 3352–3174 cm⁻¹ due to uracil moiety, and the C≡N group showed bands at 2250 cm⁻¹, carbonyl group at 1650 cm⁻¹ and more CH stretching vibration at 2990 cm⁻¹ for uracil and glycoside ring, also the MDAP(5) showed a wide range in OH vibration in 3455–3400 cm⁻¹, and more bands for NH and NH₂ which take the wide range in 3364–3175 cm⁻¹ for amino pyrazole and uracil rings and cyano group is absent and there is more bending vibration for MDAU(4) and MDAP(5) for CH aliphatic of glucose and uracil and change the vibration of aldehyde cellulose.

SEM analysis

Additionally, SEM examination of cellulose aldehyde presented the tight bundles crossed to each other and it changed the morphology of cellulose due to the oxidation process as shown in Fig. 3A Furthermore, the reaction of MDAC(2) with uracil acetamide showed cracks on the surface of cellulose due to presence of more hydrogen bonds of NH and OH groups as showed in Fig. 3B and these cracks which bonded to each other's again when reacted NH₂NH₂ to gave the pyrazole displayed its surface as the bundles collect to its self MDAP(5) as seen in Fig. 3C.

Biological activities

Anti-cancer activity

Uracil pyrazole cellulose compound was investigated on the cell growth from two tumor cells (**A549** and **Caco2**) at (6.25, 12.5, 25, 50, 100, and 200 μM) concentrations via neutral red uptake analysis which is constructed on the ability of viable cells to include and bind the supravital dye neutral red in the lysosomes. Doxorubicin (Dox) was used as a standard drug with IC₅₀ values of 4.8 and 22.5 μM against tested cells (**A549** and **Caco2** respectively). The use of DMSO as a solvent had an insignificant effect on the viability of **A549** and **Caco2** cells when preserved for 48 h. Compared with control values, all heterocycles meaningfully affected cell growth inhibition. Data in Table 2 and Fig. 4 exposed that the cytotoxic activity of the heterocycles was in the descendant order of synthesized heterocycles MDAU(4) > MDAC(2) > MDAP(5) against **A549** cancer cells. At 48 h, compounds

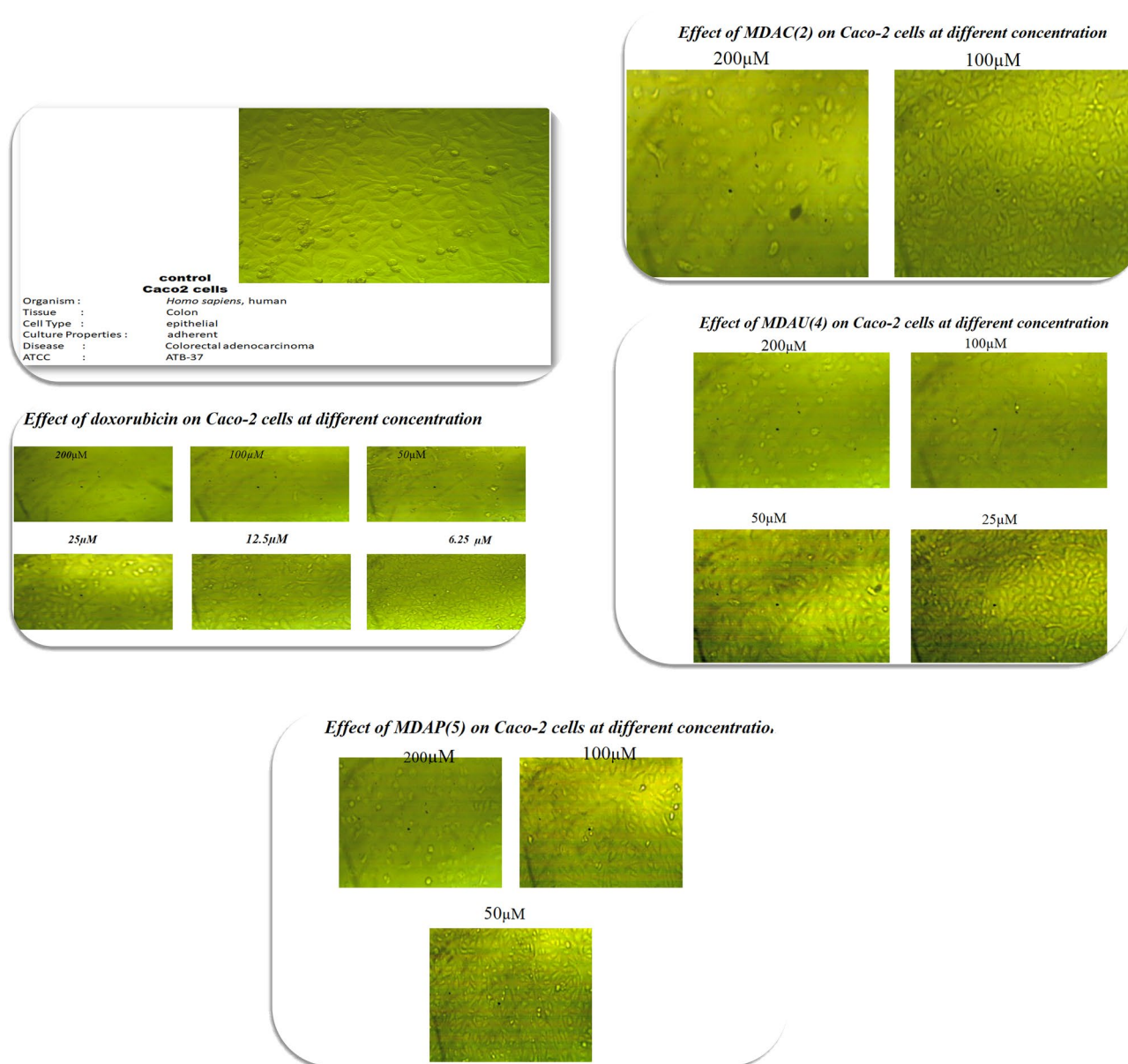


Figure 5. Effect of uracil pyrazole cellulose on **Caco2** cells with different concentrations.

MDAU(4) (17.3 μM) showed more inhibitory effects compared with starting **MDAC(2)** (59 μM) while compound **MDAP(5)** (89.7 μM) exerted a slight cytotoxic influence on **A549** cells comparable with control values. Results explained in Fig. 5 presented a middling percentage of the toxicity of **Caco2** tumor cells preserved with different concentrations of cellulose compounds after 48 h. All data in Table 2 and Fig. 5 revealed that the cytotoxic activity from the highest to the lowest is as follows compound **MDAU(4)** > **MDAP(5)** > **MDAC(2)** contra **Caco2** cells. The treatment of **Caco2** cells with compounds **MDAU(4)** (89.26 μM) exhibited high cytotoxic activity as comparable with **MDAC(2)** (188.8 μM) after 48 h. Additionally, **MDAP(5)** with IC_{50} values of (150.24 μM) displayed moderate inhibition growth than **MDAC(2)** against **Caco2** tumor cells in comparison with control values. Lastly, these outcomes exhibited that the cellulosic compounds **MDAU(4)** revealed more inhibitory effect compared to starting material and standard values once preserved with two tumor cells (**A549** and **Caco2**) after 48 hours^{43,44}.

SAR investigation

SAR examination showed the activity of the combination of heterocyclic moieties with cellulose compounds participated in variation in the cytotoxic effect of these compounds. At 48 h incubation time, The presence of dioxo tetrahydropyrimidinyl hydroxyl butenamido moiety in compound **MDAU(4)** is more effective and more cytotoxic than the presence of pyrimidinyl pyrazole carboxamide ring in **MDAP(5)** compared to the presence of dimethyl amino oxopentenenitrile ring in starting compound **MDAC(2)** when treated with **A549** and **Caco2** cells. These outcomes recognized the importance of the presence of uracil pyrazoles cellulosic compounds for anticancer activity as displayed in Fig. 6^{45,46}.

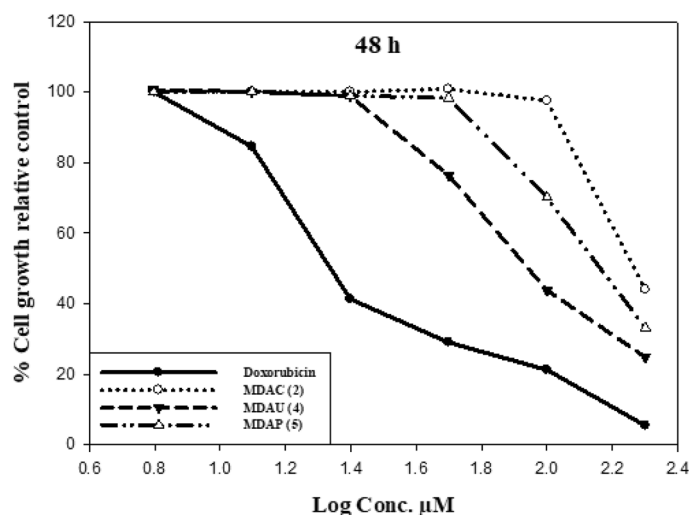


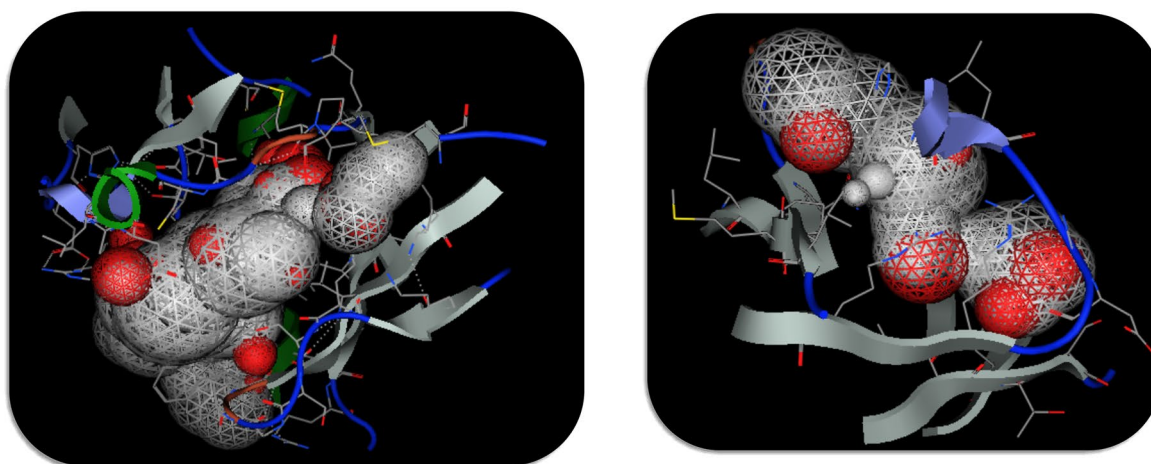
Figure 6. Effect of cellulosic compounds on Caco2 cells at 48 h.

PDBID:2ITO				PDBID:1NUN			
	Affinity of Energy (kcal/mol)	Distance (Å)	Amino acids		Affinity of Energy (kcal/mol)	Distance (Å)	Amino acids
MDAC(2)	-9.84	2.1, 2.74 Å	Thr 751, Glu 749, Thr 785, Ser784, Glu 746	MDAC(2)	-8.9231	2.41,2.57,2.87 Å	Tyr A177, Lys A 195,Gln A175
MDAU(4)	-10.325	1.72, 2.51 Å	Glu 746, Lys 714, Gln 787, Glu 709, Thr 783, Glu 749, Thr 751	MDAU(4)	-9.612	2.48, 2.66 Å	Lys A153, Arg A135, Gln A175, Arg A174, Arg A1974
MDAP(5)	-10.052	1.58,2.61,2.73,2.89 Å	Tyr 727, Lys 714, Glu 746, Glu 749	MDAP(5)	-8.524	2.47, 2.59, 2.85, 3.06 Å	Lys A1975, Lys A153, Arg A155, Gln A175, Tyr A177, Arg A193

Table 3. Docking analysis with PDBID:2ito and 1nun.

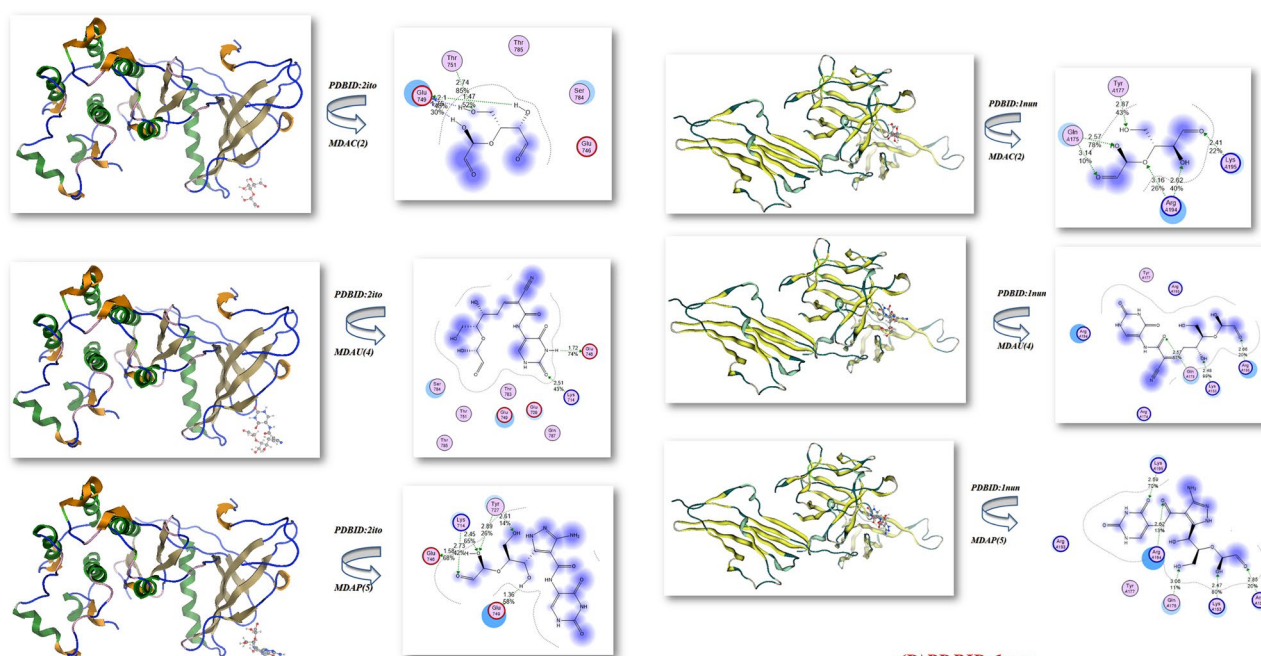
Antitumor docking analysis

Moreover, the docking simulation of uracil pyrazole cellulose was improved with bond lengths in Å units via the Moe program^{30,47}. The less energies were then executed to preserve the geometrical optimization and systematic inquiries with an RMS gradient of 0.01 Å. Crystal structure of EGFR kinase domain G719S mutation in complex with Iressa (PDBID:2ito)³¹, crystal structure analysis of the FGF10-FGFR2b Complex (PDBID:1nun)³² as demonstrated which were occupied from protein data bank in Table 3 and Fig. 7. The active site of PDBID:2ito showed 95 sides and different residues of amino acids such as (Lys 716, Leu 718, Ser 719, Ser 720, Gly 721, Ala 722, Phe 723, Gly 724, Val 726, Lys 728, Ala 743, Ile 744) as showed in Fig. 7A, and the active site in protein PDBID:1nun showed 39 sides attached with amino acids such as (His 72, Leu 73, Gly 75, Asp 76, Arg 78, Arg 80, Ile 113, Thr 114, Ser 115, Glu 154, Ile 156, Gly 160, Asn 162, Leu 202, Pro 203) as displayed in Fig. 7C. In this docking simulation, some researchers have used in silico docking and catalytic site residue analysis to successfully identify and study the enzymes used in cellulose derivatives. In Fig. 7B the interaction between synthesized cellulosic derivatives with PDBID:2ito which showed excellent binding affinity MDAU(4) with -10.325 kcal/mol and length distance (1.72, 2.51 Å) and attached amino acids (Glu 746, Lys 714, Gln 787, Glu 709, Thr 783, Glu 749, Thr 751), which is attached with N and C=O of uracil moiety, then the MDAP(5) showed -10.052 kcal/mol and it showed the least distance 1.58, 2.61, 2.73, 2.89 Å (Tyr 727, Lys 714, Glu 746, Glu 749) due to presence of more NH groups which increase its interaction and electrostatic hydrogen bond interaction, while the MDAC(2) showed least binding affinity with -9.84 kcal/mol and high length(2.1, 2.74 Å)Thr751, Glu 749, Thr 785, Ser 784, Glu 746 and this result due to absence of chelating site of NH or C=O of uracil which increase the binding efficiency site. Moreover, the docking simulation of cellulosic compounds with PDBID:1nun also showed the most reactivity of the binding site of MDAU(4) with -9.612 kcal/mol, and bond lengths 2.51 Å and displayed different interaction with amino acids through electrostatic hydrogen bond interaction (Lys A153, Arg A135, Gln A175, Arg A174, Arg A1974). Furthermore, the MDAP(5) showed moderate activity in both proteins with energy -8.524, -10.052 kcal/mol; respectively for PDBID:2ito and 1nun and bond length 1.58–3.06 Å with amino acids (Thr751, Glu 749, Thr 785, Ser 784, Glu 746), (Tyr 727, Lys 714, Glu 746, Glu 749), (Tyr A177, Lys A195, Gln A175) and (Lys A1975, Lys A153, Arg A155, Gln A175, Tyr A177, Arg A193) which showed most interaction from OH of glucose of the cellulosic chain as presented in Fig. 7D.



(A) Active Site of PDBID:2ito

(C) Active Site of PDBID:1nun



(B) PDBID:2ito

(D) PDBID:1nun

Figure 7. (A–D) Graphs of docking of active site and uracil pyrazole cellulosic with PDBID:2ito and PDBID:1nun; respectively.

From the above results, we concluded that the presence of uracil acetamide attached to cellulosic moiety increased the electrostatic hydrogen interaction and presence of NH, C=O enhanced this activity, and the presence of pyrazole uracil cellulosic derivatives enhanced the biological evaluation and docking result confirmed the biological evaluation.

Molecular studies

The impact of A549 cells preserved with uracil pyrazole cellulose MDAC(2), MDAU(4), MDAP(5) on mRNA expression levels β -Catenin, *c-Myc*, *Cyclin D1*, and *MMP7* genes were estimated utilizing IC₅₀ values of these heterocycles after 48 hours and were estimated through calculating the percentage of its expression to that of β -Actin and in comparison to control values. From earlier analysis, it is fit recognized that the expression levels of β -Catenin, *Myc*, *Cyclin D1*, and *MMP7* are up-regulated in A549 cells^{48,49}. The Wnt signaling pathway is a complex pathway that regulates cell growth and proliferation⁵⁰. The abnormal excitation of the pathway due to genetic mutation or increased stability can activate the abnormal expression of downstream target genes, including, *c-Myc*, *Cyclin*, and *MMP-7*, which can lead to cell proliferation, inhibition of cell apoptosis, and tumor formation⁵¹. Canonical Wnt/ β -catenin pathway stimulates gene transcription through β -catenin^{48,52}. MYC proto-oncogene amplification is closely related to tumor formation, development, and metastasis and is highly expressed

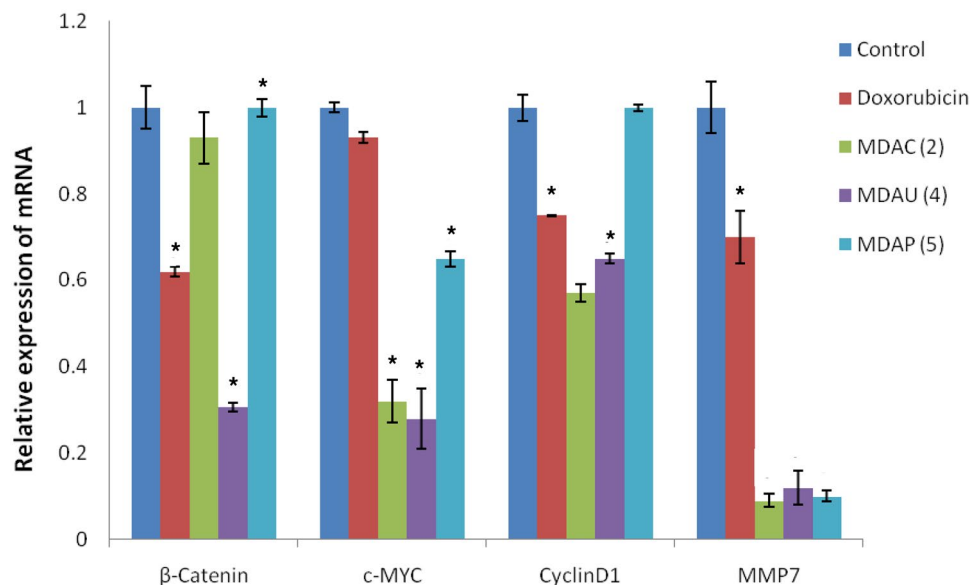


Figure 8. Effect of Doxorubicin, MDAC(2), MDAU(4) and MDAP(5) on levels of β -Catenin, c-Myc, Cyclin D1 and MMP7 genes in A549 cells. Data are represented as mean \pm SEM, Data were reproducible, * $P < 0.05$.

in cervical cancer, breast cancer, gastric cancer, and other tumors⁴¹. Cyclin D1 considerably contributed to the development of the G1 to S phase^{10,53}. The previous studies showed that the MMP-7 expression has been closely associated with tumor invasion and metastasis^{5,10,41,54}. The current results showed that doxorubicin decreased significantly the expression levels of β -Catenin, Cyclin D1, and MMP7 genes in A549 cells as compared to control values (Fig. 8). On the other hand, treatment of A549 cells with compounds MDAC(2) and MDAP(5) resulted in a significant reduction in levels of MMP7 and c-MYC genes in comparison with control values. Besides, compound MDAU(4) exhibited a significant reduction in levels of β -Catenin, c-Myc, Cyclin D1, and MMP7 genes in A549 cells compared to control values (Fig. 8). From obtained results, we found that compound MDAU(4) is the most promising anticancer agent against A549 cancer cells through the reduction of expression levels of β -Catenin, c-Myc, Cyclin D1, and MMP7 genes compared to control values^{41,50}.

Genetics docking calculation

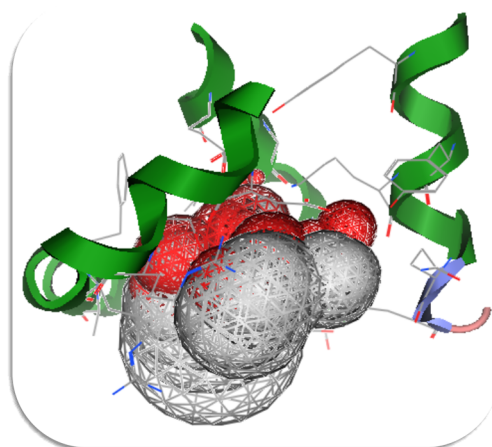
Additionally, uracil pyrazole cellulosic were interact with two types of proteins, particularly for genes for instance Bcl2-inhibitor complex PDBID: (5jsn)³³ and Crystal structure of the Skp1-FBXO31-cyclin D1 complex PDBID: (5vzu)³⁴; respectively, Figure 9A–D and Table.4,

The docking analysis of PDBID:5jsn showed 50 sides with different residues (Tyr 18, TYP 21, LYS22, Gln 25, Arg 26, GLY101, Asp102, SER 105, ARG 106, ARG 109, PHE 112, ALA113, SEP 116, GLU52) which is uracil pyrazole cellulosic displayed excellent outcome with MDAU(4) with high binding with -9.412 eV and shortage bond length (2.9, 2.76 Å) and dissimilar amino acids (Ser205, Arg 107, Gly 145, Leu 201, Trp 144, Pro 204) and the MDAP(5) showed -8.724 kcal/mol and its length (1.91, 2.75, 2.68, 2.9 Å) and linked with (Arg 106, Ser 105, Lys 22, Asp 102, Tyr 21, Gln 25, Gln 99, Tyr 202, Glu 209) which attached with OH and C=O and MDAC(2) showed least binding affinity with -8.32 kcal/mol with 1.67, 1.69, 2.81 Å and amino acids Lys 22, Gln 25, Asp 102, Arg 26 which indicate the presence of these cellulosic heterocyclic inside the pocket of protein. Moreover, the interaction of cellulosic heterocyclic with PDBID:5vzu showed 75 sides of reactivity with amino acids (Leu 29, Leu 32, THR 39, LYS 42, PHE 43, ASP44, ARG 45, HIS 64, THR 67) (Fig. 9c) which most action with MDAP(5) with -10.5147 kcal/mol and shortage length (1.42, 2.44, 1.68, 2.32 Å) and different acids Glu 1133, Arg 1154, Arg 1136, Glu 1150, Glu 1161, Cys 1160, Pro 1132 and attached with regarded for OH group of glycoside ring and C=O, NH of uracil and NH₂ of pyrazole ring as demonstrated in Fig. 9D, while MDAU(4) showed moderate with -9.5651 kcal/mol and its length (1.59, 1.38 Å) Glu 1161, Glu 1150, Glu 1133, Arg 1154, Arg 1136, Phe 1145, while the MDAC(2) showed least bonded to the pocket of protein this indication that the modification of glucose linkage increase the binding affinity inside pocket of proteins and increase its stability with different amino acids as demonstrated in Fig. 9D.

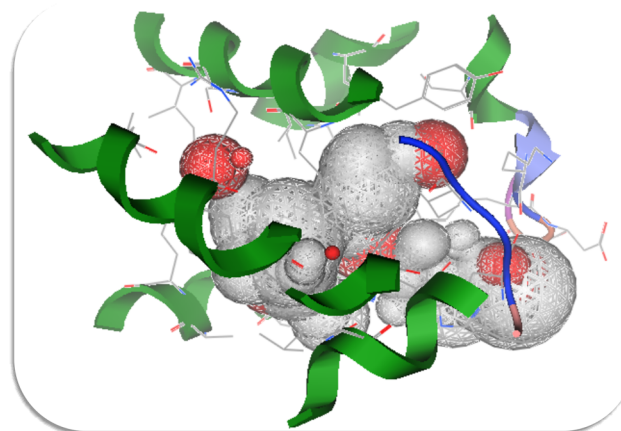
Theoretical analysis

Monomers of cellulosic heterocycles optimization

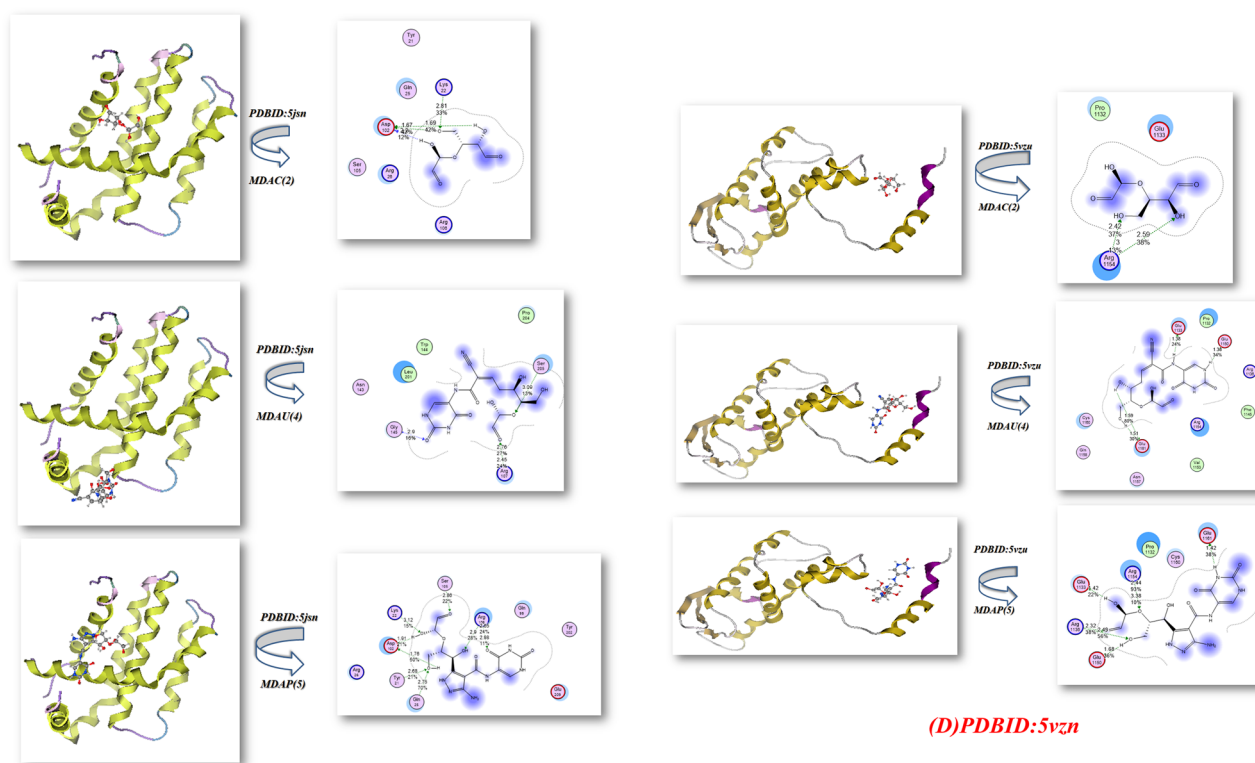
The Gaussian(09) program was used for uracil pyrazole heterocycle optimization^{36,55,56} through DFT/B3LYP/6-311(G) level. Besides, physical features of molecular structures of MDAC(2), MDAU(4), and MDAP(5) were regarding (σ) softness⁵⁷, (χ) electronegativities⁵⁸, (ΔN_{\max}) electronic charge⁵⁹, (η) hardness, (ω)⁶⁰ electrophilicity⁶¹, (S) softness⁶², and (Π) chemical potential^{63,64}, from the equations (1–8) which were listed in Table 5 and Fig. 10⁵⁹



(A) Active site of PDBID:5jsn



(C) Active site of PDBID:5vzu



(B) PDBID:5jsn

(D) PDBID:5vzu

Figure 9. (A–D): Graphs of docking stimulation of MDAC(2), MDAU(4) and MDAP(5) with different proteins.

PDBID:5jsn				PDBID:5vzu			
	Affinity of Energy (kcal/mol)	Distance(Å)	Amino acids		Affinity of Energy (kcal/mol)	Distance(Å)	Amino acids
MDAC(2)	-8.32	1.67, 1.69, 2.81 Å	Lys 22, Gln 25, Asp 102, Arg 26,	MDAC(2)	-9.1023	2.42, 2.59 Å	Glu 1133, Arg 1154, Pro 1132
MDAU(4)	-9.412	2.9, 2.76 Å	Ser205, Arg 107, Gly 145, Leu 201, Trp 144, Pro 204	MDAU(4)	-9.5651	1.59, 1.38 Å	Glu 1161, Glu 1150, Glu 1133, Arg 1154, Arg 1136, Phe 1145
MDAP(5)	-8.724	1.91, 2.75, 2.68, 2.9 Å	Arg 106, Ser 105, Lys 22, Asp 102, Tyr 21, Gln 25, Gln 99, Tyr 202, Glu 209	MDAP(5)	-10.5147	1.42, 2.44, 1.68, 2.32 Å	Glu 1133, Arg 1154, Arg 1136, Glu 1150, Glu 1161, Cys 1160, Pro 1132

Table 4. Docking uracil cellulose heterocycles with PDBID:5jsn, 5vzu.

Physical parameters	MDAC(2)	MDAU(4)	MDAP(5)
E_T (au)	-685.498	-1363.21738	-1434.5892
E_{HOMO} (eV)	-5.81811	-6.145739	-3.06756
E_{LUMO} (eV)	-1.84549	-2.75544	-2.10808
ΔE (ev)	3.97262	3.39029	0.95948
μ (Debye)	2.9272	12.1785	2.5425
χ (eV)	3.832	4.451	2.588
η (eV)	1.986	1.695	0.480
σ (eV)	0.503	0.590	2.084
Pi (eV)	-3.832	-4.451	-2.588
S (eV)	0.252	0.295	1.042
ω (eV)	3.696	5.842	6.980
ΔN max	1.9295065	2.62595	5.3916666

Table 5. Computed physical parameters for synthesized cellulosic heterocycles.

$$\Delta E = E_{LUMO} - E_{HOMO} \quad (1)$$

$$\chi = \frac{-(E_{HOMO} + E_{LUMO})}{2} \quad (2)$$

$$\eta = \frac{(E_{HOMO} - E_{LUMO})}{2} \quad (3)$$

$$\sigma = 1/\eta \quad (4)$$

$$Pi = -\chi \quad (5)$$

$$S = 1/2\eta \quad (6)$$

$$\omega = Pi^2/2 \quad (7)$$

$$\Delta N \text{ max} = -Pi/\eta \quad (8)$$

Moreover, the uracil heterocycles exhibited the non-planarity with DFT/B3LYP/6-311(G) level, and MDAC(2) showed total energy of it was (-18,653.3596 eV)(-430,156.581 kcal/mol) with coplanarity of two carbonyl group in glycoside ring and they were far of each other and blinded with each other with hydrogen bonds which make the band energy gap with $\Delta E = 3.97262$ eV and this high gap gave the aldehyde stability and ability to interact again with other compound and as demonstrated in Fig. 10A,B the delocalization of electrons in HOMO and LUMO were in all MDAC(2) and indicate of reactivity of it. Furthermore, the dipole moment of MDAC(2) showed that 2.9272D can simply for energy departure and provided it capability to react once more, its electronegativity which designated the affinity of an atom to cooperate with mutual pair of electrons exhibited a high value of 3.832 eV and its hardness and softness showed low value with 1.986 eV and 0.503; respectively and it due to ability to change its electron cloud surrounding the HC=O of aldehyde group. The Pi chemical potential of MDAC(2) gives it the capability to respond and captivate more energy in dissimilar temperature varieties and they presented -3.832 eV which gave them the capability to accumulate energy inside it. ω indicated electrophilic attractiveness and electron flow between donor and acceptor so, the MDAC(2) exhibited higher electrophilic attractiveness to captivate electrons with 3.696 eV^{65,66},

Additionally, the energy of the cellulosic compound MDAU(4) is more stable than MDAC(2) with (-37,095.0520509 eV)(-855,432.003784 kcal/mol) due to the presence of the uracil moiety connected to MDAC(2) and more NH groups, which increase the stability of the molecule^{35,42}. This is demonstrated in Fig. 9C,D. Additionally, FMO represents electron affinity and ionization potential. Additionally, the heterocycle's stability and reactivity were determined by the band gap energy. While heterocycles with a smaller band gap will be less stable and more reactive, those with a larger band gap will be more stable⁶⁷⁻⁶⁹. According to Fig. 9B, the HOMO-LUMO orbitals' energy planes and circulations were computed at the B3LYP/6-311G(d, p) level for the complex MDAU(4) on the glucose and uracil moiety in HOMO and LUMO due to more NH and OH groups, which provided it stability with a gap energy of 3.39029 eV. With a dipole moment of 12.1785D, this compound has a high dipole attraction that makes charge separation simple. Due to the presence of CN-CH=, which gives an atom the ability to respond again, practical MDAU(4) displayed a high value of 4.451 eV for its electronegativity, and similarly, the (eV) can easily change the electron charge with -4.451 eV can be easily to store more energy inside it⁷⁰⁻⁷³. Due to the formation of pyrazole attached to cellulose with (-39,037.179122 eV)

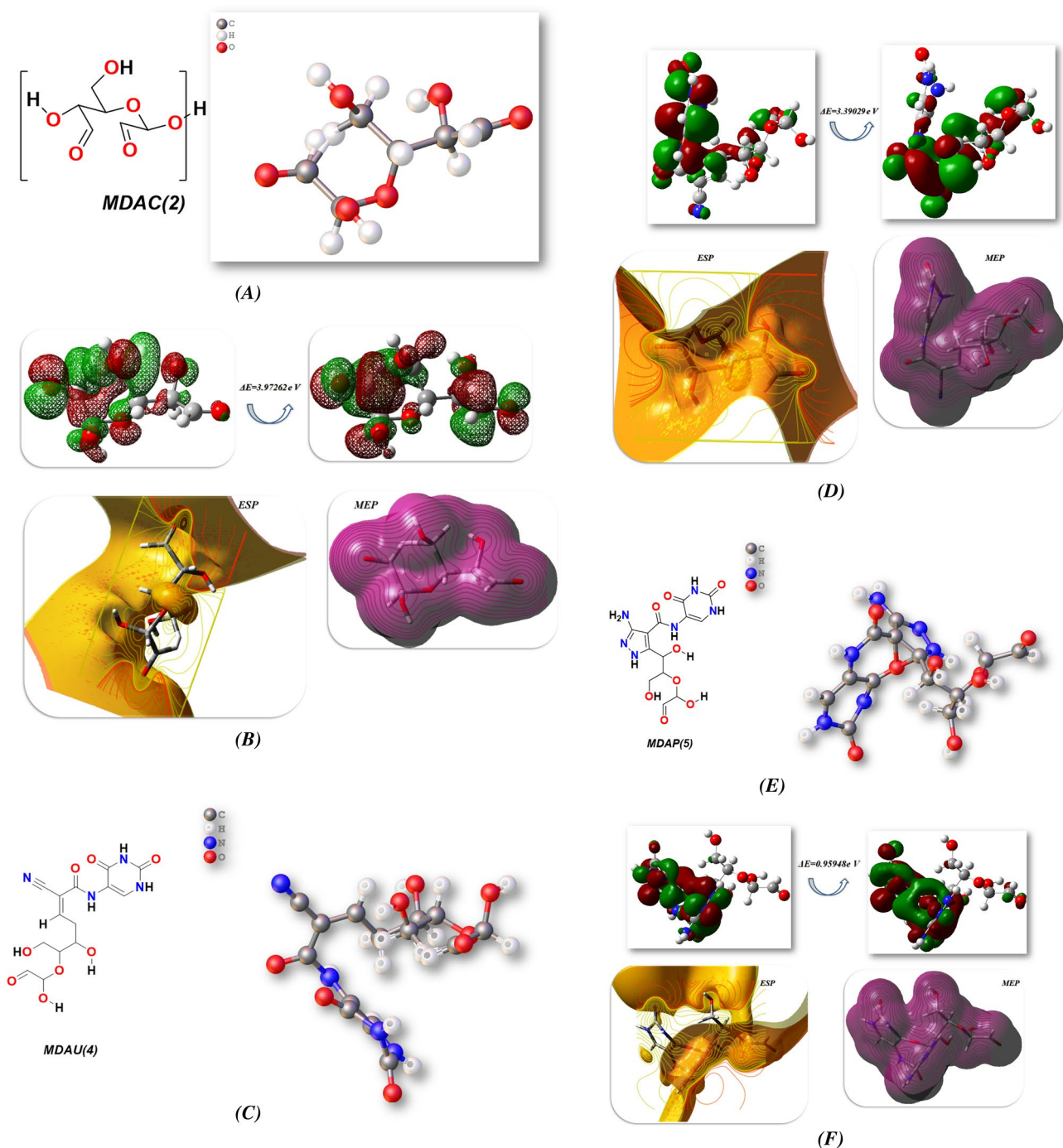


Figure 10. (A–F): FMO of an optimised chemical structure. DFT/B3LYP/6–311 (G) level was used by MDAC(2), MDAU(4), and MDAP(5) for ESP and MEP.

(–900,218.50658 kcal/mol), its HOMO–LUMO delocalization of charge on pyrazole and uracil rings and lack of delocalization on OH group of glucose ring, as well as the presence of NH and carbonyl of pyrazole uracil, the MDAP(5) demonstrated greater stability than MDAU(4), gave it stability, its band energy gap was 0.95948 eV, and the charge energy departure of its dipole moment was 2.5425D. As a result, the MDAP(5) displayed high electrophilic attractiveness with 6.980 eV and electronic charge ΔN max with 5.39 eV due to more NH and NH_2 , which increased the electronic charge^{74,75} on it as shown in Table.5 and Fig. 10(E, F).

Conclusion

In this elucidation, the cellulosic aldehyde was combined with uracil acetamide to produce the corresponding arylidene cellulosic derivatives, which served as the active site for the nucleophilic addition to give the corresponding pyrazole cellulosic derivative. These heterocycles were then confirmed through various analyses,

and it was discovered that more hydrogen bond interactions caused the binding to occur on the cellulosic surface. Additionally, the tested compound MDAU(4) displayed the lowest IC₅₀ values and the largest cytotoxic activity against A549 and Caco2 cells in comparison to the beginning compound MDAC(2)⁴⁷. And also, it was a reduced expression levels of the Wnt genes (β -Catenin, c-Myc, Cyclin D1, and MMP7) are likewise expressed at lower levels in A549 cells after 48 h. Additionally, the docking stimulation revealed that MDAU(4) had an excellent binding affinity for the majority of proteins with the least amount of energy required due to the presence of more NH and OH in its structure. These findings were further supported by the physical descriptors of these cellulosic compounds, which demonstrated the stability of these compounds due to increased hydrogen bonding interaction.

Data availability

All data generated or analyzed during this study are included in this published.

Received: 3 July 2023; Accepted: 28 August 2023

Published online: 04 September 2023

References

- Hindi, S. & Hindi, S. J. B. J. Microcrystalline cellulose: Its processing and pharmaceutical specifications. *BioCryst. J.* **1**, 26–38 (2016).
- Khodair, A. I., Kassab, S. E., Kheder, N. A. & Fahim, A. M. Synthesis of novel d- α -galactopyranosyl-l-seryl/l-threonyl-l-alanyl-l-alanine as useful precursors of new glycopeptide antibiotics with computational calculations studies. *Carbohydr. Res.* **514**, 108546. <https://doi.org/10.1016/j.carres.2022.108546> (2022).
- Dacrory, S. & Fahim, A. M. Synthesis, anti-proliferative activity, computational studies of tetrazole cellulose utilizing different homogenous catalyst. *Carbohydr. Polym.* **229**, 115537. <https://doi.org/10.1016/j.carbpol.2019.115537> (2020).
- Fahim, A. M., Hasanin, M., Habib, I. H. I., El-Attar, R. O. & Dacrory, S. Synthesis, antimicrobial activity, theoretical investigation, and electrochemical studies of cellulosic metal complexes. *J. Iran. Chem. Soc.* <https://doi.org/10.1007/s13738-023-02790-1> (2023).
- Fahim, A. M., Farag, A. M., Mermer, A., Bayrak, H. & Şirin, Y. Synthesis of novel β -lactams: Antioxidant activity, acetylcholinesterase inhibition and computational studies. *J. Mol. Struct.* **1233**, 130092. <https://doi.org/10.1016/j.molstruc.2021.130092> (2021).
- Hiorth, M., Nilsen, S. & Tho, I. Bioadhesive mini-tablets for vaginal drug delivery. *Pharmaceutics* **6**, 494–511. <https://doi.org/10.3390/pharmaceutics6030494> (2014).
- Raghav, N., Sharma, M. R. & Kennedy, J. F. Nanocellulose: A mini-review on types and use in drug delivery systems. *Carbohydr. Polym. Technol. Appl.* **2**, 100031. <https://doi.org/10.1016/j.carpta.2020.100031> (2021).
- Fahim, A. M. & Abu-El Magd, E. E. Performance efficiency of MIPOH polymers as organic filler on cellulose pulp waste to form cellulosic paper sheets with biological evaluation and computational studies. *Polym. Bull.* **79**, 4099–4131. <https://doi.org/10.1007/s00289-021-03685-y> (2022).
- Weller, D., Peake, M. & Field, J. Presentation of lung cancer in primary care. *NPJ Prim. Care Respir. Med.* **29**, 1–5 (2019).
- Fahim, A. M., Abouzeid, R. E., Kiey, S. A. A. & Dacrory, S. Development of semiconductive foams based on cellulose-benzenesulfonate/CuFe₂O₄- nanoparticles and theoretical studies with DFT/B3PW91/LANDZ2 basis set. *J. Mol. Struct.* **1247**, 131390. <https://doi.org/10.1016/j.molstruc.2021.131390> (2022).
- MacDonald, B. T., Tamai, K. & He, X. Wnt/ β -catenin signaling: Components, mechanisms, and diseases. *Dev. Cell* **17**, 9–26 (2009).
- Rogers, C. D., Sorrells, L. K. & Bronner, M. E. A catenin-dependent balance between N-cadherin and E-cadherin controls neuroectodermal cell fate choices. *Mech. Dev.* **152**, 44–56 (2018).
- Shi, X. *et al.* Wnt/ β -catenin signaling pathway is involved in regulating the migration by an effective natural compound brucine in LoVo cells. *Phytomedicine* **46**, 85–92 (2018).
- Fahim, A. M., Mohamed, A. & Ibrahim, M. A. Experimental and theoretical studies of some propiolate esters derivatives. *J. Mol. Struct.* **1236**, 130281. <https://doi.org/10.1016/j.molstruc.2021.130281> (2021).
- Pohl, S.-G. *et al.* Wnt signaling in triple-negative breast cancer. *Oncogenesis* **6**, e310–e310 (2017).
- Shang, Z. *et al.* USP9X-mediated deubiquitination of B-cell CLL/lymphoma 9 potentiates Wnt signaling and promotes breast carcinogenesis. *J. Biol. Chem.* **294**, 9844–9857 (2019).
- Klaus, A. & Birchmeier, W. Wnt signalling and its impact on development and cancer. *Nat. Rev. Cancer* **8**, 387–398 (2008).
- Magar, H. S., Magd, E.E.A.-E., Hassan, R. Y. A. & Fahim, A. M. Rapid impedimetric detection of cadmium ions using Nanocellulose/ligand/nanocomposite (CNT/Co₃O₄). *Microchem. J.* **182**, 107885. <https://doi.org/10.1016/j.microc.2022.107885> (2022).
- Yang, C.-M. *et al.* β -Catenin promotes cell proliferation, migration, and invasion but induces apoptosis in renal cell carcinoma. *Oncotargets Ther.* **10**, 711 (2017).
- Xie, X.-M. *et al.* Aberrant hypermethylation and reduced expression of disabled-2 promote the development of lung cancers. *Int. J. Oncol.* **43**, 1636–1642 (2013).
- Xu, H.-T. *et al.* Disabled-2 and Axin are concurrently colocalized and underexpressed in lung cancers. *Hum. Pathol.* **42**, 1491–1498 (2011).
- Mohamed, A., Fahim, A. M. & Ibrahim, M. A. Theoretical investigation on hydrogen bond interaction between adrenaline and hydrogen sulfide. *J. Mol. Model.* **26**, 354. <https://doi.org/10.1007/s00894-020-04602-2> (2020).
- Mohamed, A., Fahim, A. M., Ibrahim, S. A. E. & Ibrahim, M. A. Studies on hydrogen bonding of adrenaline/acetone and adrenaline/methanol complexes: Computational and experimental approach. *Struct. Chem.* **32**, 2115–2138. <https://doi.org/10.1007/s11224-021-01773-3> (2021).
- Mahmoud, N. H., Emara, A. A., Linert, W., Fahim, A. M. & Abou-Hussein, A. A. Synthesis, spectral investigation, biological activities and docking stimulation of novel metal complexes of Trifluoro phenylthiazol derivative with computational studies. *J. Mol. Struct.* **1272**, 134095 (2023).
- Fahim, A. M., Ismael, E. H. I., Elsayed, G. H. & Farag, A. M. Synthesis, antimicrobial, anti-proliferative activities, molecular docking and DFT studies of novel pyrazolo[5,1-c][1, 2, 4]triazine-3-carboxamide derivatives. *J. Biomol. Struct. Dyn.* <https://doi.org/10.1080/07391102.2021.1930582> (2021).
- Ali, A., Ganie, S. A. & Mazumdar, N. A new study of iodine complexes of oxidized gum arabic: An interaction between iodine monochloride and aldehyde groups. *Carbohydr. Polym.* **180**, 337–347 (2018).
- Guo, J., Ge, L., Li, X., Mu, C. & Li, D. Periodate oxidation of xanthan gum and its crosslinking effects on gelatin-based edible films. *Food Hydrocoll.* **39**, 243–250 (2014).
- Dacrory, S. Antimicrobial activity, DFT calculations, and molecular docking of dialdehyde cellulose/graphene oxide film against Covid-19. *J. Polym. Environ.* **29**, 2248–2260. <https://doi.org/10.1007/s10924-020-02039-5> (2021).
- Repetto, G., Del Peso, A. & Zurita, J. L. Neutral red uptake assay for the estimation of cell viability/cytotoxicity. *Nat. Protoc.* **3**, 1125–1131 (2008).

30. Vilar, S., Cozza, G. & Moro, S. Medicinal chemistry and the molecular operating environment (MOE): Application of QSAR and molecular docking to drug discovery. *Curr. Top. Med. Chem.* **8**, 1555–1572 (2008).
31. Yun, C.-H. *et al.* Structures of lung cancer-derived EGFR mutants and inhibitor complexes: Mechanism of activation and insights into differential inhibitor sensitivity. *Cancer Cell* **11**, 217–227 (2007).
32. Yeh, B. K. *et al.* Structural basis by which alternative splicing confers specificity in fibroblast growth factor receptors. *Proc. Natl. Acad. Sci.* **100**, 2266–2271 (2003).
33. Berger, S. *et al.* Computationally designed high specificity inhibitors delineate the roles of BCL2 family proteins in cancer. *elife* **5**, e20352 (2016).
34. Li, Y. *et al.* Structural basis of the phosphorylation-independent recognition of cyclin D1 by the SCFFBXO31 ubiquitin ligase. *Proc. Natl. Acad. Sci.* **115**, 319–324 (2018).
35. Elsayed, G. H., Fahim, A. M. & Khodair, A. I. Synthesis, anti-cancer activity, gene expression and docking stimulation of 2-thioximidazolidin-4-one derivatives. *J. Mol. Struct.* **1265**, 133401. <https://doi.org/10.1016/j.molstruc.2022.133401> (2022).
36. Frisch, A. *gaussian 09W Reference* 25 (Wallingford, 2009).
37. Aboelnaga, A., Fahim, A. M. & El-Sayed, T. H. Computer aid screening for potential antimalarial choroquinone compounds as Covid 19 utilizing computational calculations and molecular docking study. *OnLine J. Biol. Sci.* <https://doi.org/10.3844/ojbsci.2020.207.220> (2020).
38. Aboelnaga, A., Mansour, E., Fahim, A. M. & Elsayed, G. H. Synthesis, anti-proliferative activity, gene expression, docking and DFT investigation of novel pyrazol-1-yl-thiazol-4(5H)-one derivatives. *J. Mol. Struct.* **1251**, 131945. <https://doi.org/10.1016/j.molstruc.2021.131945> (2022).
39. Dennington, R., Keith, T. & Millam, J. GaussView, Version 4.1. 2. *Semichem Inc., Shawnee Mission, KS* (2007).
40. El-Ayaan, U., El-Metwally, N. M., Youssef, M. M. & El Bialy, S. A. Perchlorate mixed-ligand copper(II) complexes of β -diketone and ethylene diamine derivatives: thermal, spectroscopic and biochemical studies. *Spectrochim. Acta Part A Mol. Biomol. Spectrosc.* **68**, 1278–1286 (2007).
41. Tolan, H. E. M., Fahim, A. M. & Ismael, E. H. I. Synthesis, biological activities, molecular docking, theoretical calculations of some 1,3,4-oxadiazoles, 1,2,4-triazoles, and 1,2,4-triazolo[3,4-b]-1,3,4-thiadiazines derivatives. *J. Mol. Struct.* **1283**, 135238. <https://doi.org/10.1016/j.molstruc.2023.135238> (2023).
42. Attia, A., Aboelnaga, A. & Fahim, A. M. Isonicotinohydrazide chalcone and Its Ni complex as corrosion inhibitors during acid cleaning: Theoretical and experimental approaches. *Egypt. J. Chem.* **66**(7), 95–111 (2023).
43. Kumar, V., Singh, R. K., Kumari, V., Kumar, B. & Sharma, S. Studies of distorted octahedral complexes of cobalt, nickel and copper and their antibacterial properties. *Orient. J. Chem.* **34**, 1937 (2018).
44. Fahim, A. M., Elshikh, M. S. & Darwish, N. M. Synthesis, antitumor activity, molecular docking and DFT study of novel pyrimidopyrazole derivatives. *Curr. Comput. Aided Drug Des.* **16**, 486–499 (2020).
45. Nanjundan, N. *et al.* Distorted tetrahedral bis-(N,S) bidentate Schiff base complexes of Ni(II), Cu(II) and Zn(II): Synthesis, characterization and biological studies. *Polyhedron* **110**, 203–220 (2016).
46. Fahim, A. M. & Shalaby, M. A. Synthesis, biological evaluation, molecular docking and DFT calculations of novel benzenesulfonamide derivatives. *J. Mol. Struct.* **1176**, 408–421 (2019).
47. Fahim, A. M. Anti-proliferative activity, molecular docking study of novel synthesized ethoxyphenylbenzene sulfonamide with computational calculations. *J. Mol. Struct.* **1277**, 134871. <https://doi.org/10.1016/j.molstruc.2022.134871> (2023).
48. Shalaby, M. A., Fahim, A. M. & Rizk, S. A. Antioxidant activity of novel nitrogen scaffold with docking investigation and correlation of DFT stimulation. *RSC Adv.* **13**, 14580–14593. <https://doi.org/10.1039/D3RA02393A> (2023).
49. Tolan, H. E. M., Fahim, A. M. & Ismael, E. H. I. Synthesis, chemical characterization, and anti-proliferative action of 1,2,4-triazole N-glycoside derivatives. *Egypt. J. Chem.* <https://doi.org/10.21608/ejchem.2023.217561.8139> (2023).
50. El-Shall, F. N., Fahim, A. M. & Dacrory, S. Making a new bromo-containing cellulosic dye with antibacterial properties for use on various fabrics using computational research. *Sci. Rep.* **13**, 10066. <https://doi.org/10.1038/s41598-023-36688-y> (2023).
51. Shalaby, M. A., Rizk, S. A. & Fahim, A. M. Synthesis, reactions and application of chalcones: A systematic review. *Org. Biomol. Chem.* <https://doi.org/10.1039/D3OB00792H> (2023).
52. Shalaby, M. A., Rizk, S. A. & Fahim, A. M. Synthesis, reactions and application of chalcones: A systematic review. *Org. Biomol. Chem.* **21**, 5317–5346. <https://doi.org/10.1039/D3OB00792H> (2023).
53. Asmaa M. Fahim, Ahmad M. Farag, Synthesis, antimicrobial evaluation, molecular docking and theoretical calculations of novel pyrazolo[1,5-a]pyrimidine derivatives. *J. Molecular Structure* **1199**, 127025. <https://doi.org/10.1016/j.molstruc.2019.127025> (2020).
54. Fahim, A. M., Magar, H. S., Nasar, E., Abdelrazek, F. M. & Aboelnaga, A. Synthesis of Cu-porphyrazines by annulated diazepine rings with electrochemical, conductance activities and computational studies. *J. Inorg. Organomet. Polym. Mater.* **32**, 240–266. <https://doi.org/10.1007/s10904-021-02122-x> (2022).
55. Fahim, A. M. & Shalaby, M. A. Synthesis, biological evaluation, molecular docking and DFT calculations of novel benzenesulfonamide derivatives. *J. Mol. Struct.* **1176**, 408–421 (2019).
56. Fahim, A. M., Magar, H. S., Mahmoud, N. H. Synthesis, antimicrobial, antitumor activity, docking simulation, theoretical studies, and electrochemical analysis of novel Cd(II), Co(II), Cu(II), and Fe(III) complexes containing barbituric moiety. *Appl Organomet. Chem* **37**(4), e7023. <https://doi.org/10.1002/aoc.7023> (2023).
57. Chattaraj, P. K., Cedillo, A. & Parr, R. G. Chemical softness in model electronic systems: Dependence on temperature and chemical potential. *Chem. Phys.* **204**, 429–437 (1996).
58. Asmaa M. Fahim, Ehab E. Abu-El Magd, Enhancement of Molecular imprinted polymer as organic fillers on bagasse cellulose fibers with biological evaluation and computational calculations, *J. Molecular Structure*, **1241**, 130660. <https://doi.org/10.1016/j.molstruc.2021.130660> (2021).
59. Livak, K. J. & Schmittgen, T. D. Analysis of relative gene expression data using real-time quantitative PCR and the $2^{-\Delta\Delta C_T}$ method. *Methods* **25**(4), 402–408. <https://doi.org/10.1006/meth.2001.1262> (2001).
60. Parr, R. G. & Pearson, R. G. Absolute hardness: Companion parameter to absolute electronegativity. *J. Am. Chem. Soc.* **105**, 7512–7516 (1983).
61. Fahim, A. M., Shalaby, M. A. & Ibrahim, M. A. Microwave-assisted synthesis of novel 5-aminouracil-based compound with DFT calculations. *J. Mol. Struct.* **1194**, 211–226. <https://doi.org/10.1016/j.molstruc.2019.04.078> (2019).
62. Domingo, L. R., Aurell, M. J., Pérez, P. & Contreras, R. Quantitative characterization of the global electrophilicity power of common diene/dienophile pairs in Diels-Alder reactions. *Tetrahedron* **58**, 4417–4423 (2002).
63. Vela, A. & Gazquez, J. L. A relationship between the static dipole polarizability, the global softness, and the fukui function. *J. Am. Chem. Soc.* **112**, 1490–1492 (1990).
64. Yıldız Uygün Cebeci, Hacer Bayrak, Şengül Alpay Karaoğlu, Asmaa M. Fahim, Synthesis of novel antipyrene-azole-S-alkyl derivatives antimicrobial activity, molecular docking, and computational studies. *J. Molecular Structure* **1260**, 132810. <https://doi.org/10.1016/j.molstruc.2022.132810> (2022).
65. Elsayed, G. H., Dacrory, S. & Fahim, A. M. Anti-proliferative action, molecular investigation and computational studies of novel fused heterocyclic cellulosic compounds on human cancer cells. *Int. J. Biol. Macromol.* **222**, 3077–3099. <https://doi.org/10.1016/j.ijbiomac.2022.10.083> (2022).

66. Fahim, A. M., Ghabbour, H. A., Kabil, M. M., Al-Rashood, S. T. & Abdel-Aziz, H. A. Synthesis, X-ray crystal structure, Hirshfeld analysis and computational investigation of bis(methylthio)acrylonitrile with antimicrobial and docking evaluation. *J. Mol. Struct.* **1260**, 132793. <https://doi.org/10.1016/j.molstruc.2022.132793> (2022).
67. Ghabbour, H. A., Fahim, A. M., Abu El-Enin, M. A., Al-Rashood, S. T. & Abdel-Aziz, H. A. Crystal structure, Hirshfeld surface analysis and computational study of three 2-(4-arylthiazol-2-yl)isoindoline-1,3-dione derivatives. *Mol. Cryst. Liq. Cryst.* **742**, 40–55. <https://doi.org/10.1080/15421406.2022.2045794> (2022).
68. Kohn, W., Becke, A. D. & Parr, R. G. Density functional theory of electronic structure. *J. Phys. Chem.* **100**, 12974–12980. <https://doi.org/10.1021/jp960669l> (1996).
69. Akl, E.M., Dacrory, S., Abdel-Aziz, M.S. et al. Preparation and characterization of novel antibacterial blended films based on modified carboxymethyl cellulose/phenolic compounds. *Polym. Bull.* **78**, 1061–1085. <https://doi.org/10.1007/s00289-020-03148-w> (2021).
70. Fahim, A. M., Ismael, E. H., Elsayed, G. H. & Farag, A. M. Synthesis, antimicrobial, anti-proliferative activities, molecular docking and DFT studies of novel pyrazolo [5, 1-c][1, 2, 4] triazine-3-carboxamide derivatives. *J. Biomol. Struct. Dyn.* **40**(19), 9177–93 (2021).
71. Asmaa M. Fahim, Hala. E.M. Tolan, Wael A. El-Sayed, Synthesis of novel 1,2,3-triazole based acridine and benzothiazole scaffold N-glycosides with anti-proliferative activity, docking studies, and comparative computational studies. *J. Molecular Structure* **1251**, 131941. <https://doi.org/10.1016/j.molstruc.2021.131941> (2022).
72. Kheder, A. et al. Synthesis and in-silico studies of some new thiazole carboxamide derivatives with theoretical investigation. *Polycycl. Aromat. Compd.* <https://doi.org/10.1080/10406638.2023.2243639> (2023).
73. Farag, A. M., Kheder, N. A., Fahim, A. M. & Dawood, K. M. Regioselective synthesis and computational calculation studies of some new pyrazolyl-pyridine and bipyridine derivatives. *J. Heterocycl. Chem.* <https://doi.org/10.1002/jhet.4705> (2023).
74. Bayrak, H. et al. Synthesis, antioxidant activity, docking simulation, and computational investigation of novel heterocyclic compounds and Schiff bases from picric acid. *J. Mol. Struct.* **1281**, 135184. <https://doi.org/10.1016/j.molstruc.2023.135184> (2023).
75. Fahim, A. M. et al. Synthesis and DFT calculations of aza-Michael adducts obtained from degradation poly (methyl methacrylate) plastic wastes. *Int. J. Environ. Waste Manag.* **24**, 337–353 (2019).

Acknowledgements

The authors acknowledge the (NRC) National Research Centre.

Author contributions

A.M.F: software, synthesis, validation, formal analysis, resources, data curation, software, formal analysis, investigation, resources, writing—original draft and review it, supervision; S.D: data curation, methodology of cellulose aldehyde; G.H.E; conceptualization, writing—review and editing, visualization of biological activity.

Funding

Open access funding provided by The Science, Technology & Innovation Funding Authority (STDF) in cooperation with The Egyptian Knowledge Bank (EKB).

Competing interests

The authors declare no competing interests.

Additional information

Correspondence and requests for materials should be addressed to A.M.F.

Reprints and permissions information is available at www.nature.com/reprints.

Publisher's note Springer Nature remains neutral with regard to jurisdictional claims in published maps and institutional affiliations.



Open Access This article is licensed under a Creative Commons Attribution 4.0 International License, which permits use, sharing, adaptation, distribution and reproduction in any medium or format, as long as you give appropriate credit to the original author(s) and the source, provide a link to the Creative Commons licence, and indicate if changes were made. The images or other third party material in this article are included in the article's Creative Commons licence, unless indicated otherwise in a credit line to the material. If material is not included in the article's Creative Commons licence and your intended use is not permitted by statutory regulation or exceeds the permitted use, you will need to obtain permission directly from the copyright holder. To view a copy of this licence, visit <http://creativecommons.org/licenses/by/4.0/>.

© The Author(s) 2023, corrected publication 2024